

Effect of montmorillonite on the morphologies and properties of monomer casting polyamide 6/polystyrene blends via successive in situ polymerization

Yan Liu · Zhenming Chen · Tingxiu Xie · Guisheng Yang

Received: 1 September 2010 / Accepted: 2 December 2010 / Published online: 14 December 2010
© Springer Science+Business Media, LLC 2010

Abstract Monomer casting polyamide 6 (MCPA6)/polystyrene (PS)/montmorillonite (MMT) ternary composites were prepared via successive in situ polymerization. The effects of Na^+ -MMT and OMMT on morphologies of MCPA6/PS blends have been studied by scanning electron microscopy (SEM) and transmission electronic microscopy (TEM). Incorporation of certain amount of Na^+ -MMT results in the diameter of PA6 dispersed microspheres in PS matrix increased significantly from several to dozens of micrometers. It was interesting to find that all Na^+ -MMT was dispersed only in the MCPA6 microspheres. However, a different morphology was observed in MCPA6/PS blend with incorporation of OMMT, especially when the content of OMMT ≥ 1 wt%. That is, the morphologies of the ternary blends change from dispersed PA6 microspheres/PS matrix to dispersed PA6 network with inclusion of local PA6 microspheres/PS matrix. It was surprising that OMMT dispersed in PA6 microspheres at low OMMT loading (i.e., 0.5 wt%), while OMMT was dispersed in PA6 network phase, not in PA6 microspheres phase at high OMMT loading (i.e., ≥ 1 wt%). The incorporation of a various amount of MMT affected the crystallization behavior of PA6 phase in the MCPA6/PS blends by the results of XRD and DSC. The MMT layers leaded to the co-existence of α -crystalline form and γ -crystalline form of PA6. Furthermore, the more the MMT contents, the stronger the intensity of the γ -peak. Another

interesting phenomenon was that there was a remarkable difference in molecular weight of PA6 microspheres phase and PA6 network phase in MCPA6/PS/OMMT (2 wt%) ternary composites from GPC results.

Introduction

Polymer blends are known to be a very economic route for extending the applications of materials. Clay has been used as an alternative route to manipulate the interfacial properties of a variety of polymer blends over the past several decades [1–6]. A good deal of study focuses on improving the performance of composites or studying the morphology and compatible effect of clay in the immiscible polymer blends. When clay is added into polymer blends, what the key issue to be considered is the location of clay, which may affect the morphology and properties of the immiscible blends or the compatible influence of composites [7–11]. The clay has preferential intercalation behavior with tendency to disperse in a certain phase or in the interphase of polymer blends [12]. Polyamide 6 (PA6) is an important group of the thermoplastic with excellent properties [13–15]. Among plentiful polymer pairs, preparation for blends of polyamide 6 (PA6)/Polystyrene (PS) have received great success. Owing to the intrinsically different polarities of PA6 and PS, the blends are immiscible and represent two-phase morphology with poor interfacial adhesion [16, 17]. In those literatures, PA6/PS blends are usually prepared by melt-mixing method to form PS dispersed/PA6 matrix structure [18–22]. However, polymerization of the reactive solvent in solution of polymer/reactive solvent is another method to fabricate polymer blends. It can demonstrate completely dissimilar morphologies compared with that of conventional method.

Y. Liu · Z. Chen · G. Yang (✉)
Department of Polymer Science and Engineering,
Zhejiang University, 310027 Hangzhou, Zhejiang, China
e-mail: ygs20082008@gmail.com

T. Xie · G. Yang
Shanghai Genius Advanced Materials Co., Ltd,
201109 Shanghai, China

Recently, a reactive solvent method above-mentioned for the PA6/PS blends was developed in our group via successive in situ polymerization of the styrene (free radical polymerization) and ϵ -caprolactam monomers (anionic ring-opening polymerization) in one reactor [23]. It is surprising that when the PS content is higher than 15 wt%, phase inversion starts up, PA6 microspheres are observed. PA6 microspheres is an attractive carrier and thus has great potential in bioengineering involving protein (or enzyme) immobilization because of the same functional bond namely amide in their main chains [24–28]. Furthermore, PA6 microspheres are of particular interest from commercial viewpoint.

Thus, the objective of this study is to investigate the effects of pristine Na⁺-MMT and organic MMT on the morphologies and properties of PA6 microspheres in the MCPA6/PS blends via successive in situ polymerization. An attempt has been made to understand the relationship between morphologies and dispersion of MMT in MCPA6/PS blends. At the same time, the work should contribute to achieving a basic knowledge of the further development of commercial PA6 microspheres.

Experiments parts

Materials and sample preparation

ϵ -Caprolactam monomer (CL) was bought from Nanjing Oriental Chemical Company (Commercial-grade, China). Azodiisobutyronitrile (AIBN), Dimethylacetamide (DMAC), Tetrahydrofuran (THF), Sodium hydroxide (NaOH), and 2,4-toluene diisocyanate (TDI) (Analysis purity) used in this study were all purchased from Shanghai Chemical Reagents Co. and used without further treatment. Styrene was distilled at 45 °C under vacuum and reserved at –20 °C. Na⁺-MMT (PGV) with a cation-exchange capacity (CEC) of 145 mequiv. Per 100 g and OMMT (I.44P) were all supplied by Nanocor Co., Ltd (America), and dried in the vacuum at 80 °C for 24 h before use.

MCPA6/PS/MMT ternary composites were prepared following the two steps below:

- (1) Styrene was dispersed in melted ϵ -caprolactam monomer at 80 °C with the weigh ratio of 20/80, and a homogeneous transparent mixture was observed. Then 0.2 wt% AIBN was added and kept stirred for 24 h at 80 °C for the polymerization of styrene. After it, a clear and viscous mixture PS/CL was obtained.
- (2) Na⁺-MMT or OMMT was added to the above mentioned mixture after being ultrasounding for 24 h using DMAC solvent for pre-dispersed. The mixture

was vacuumed at 120 °C for several hours to remove residual DMAC and styrene monomer. After this, 0.4 wt% NaOH was added, and vacuumed at 120 °C for 20 min to remove trace amount of water and then 0.4 wt% TDI was added with stirring. The mixture was immediately poured into a mold preheated to 160 °C and polymerized in oven at 160 °C for 20 min. Binary PA6/PS blend was synthesized under the same reaction conditions as above without adding MMT. The composites obtained were denoted as NM0.5 (0.5 wt% Na⁺-MMT), NM1 (1 wt% Na⁺-MMT), NM2 (2 wt% Na⁺-MMT) and OM0.5 (0.5 wt% OMMT), OM1 (1 wt% OMMT), OM2 (2 wt% OMMT), and Reference (0 wt% MMT).

During the in situ compounding process, the free radical polymerization of styrene was first performed using ϵ -caprolactam as solvent, and second, the anionic ring-opening of ϵ -caprolactam was initiated in situ in the in situ prepared PS component and MMT. The treatment processes of all compositions were identical to ensure comparability and accuracy of the testing results.

Finally, all samples were crashed and etched the PS matrix with THF. PA6 microspheres with various amount of Na⁺-MMT and OMMT, and the PA6 network phase with OMMT were obtained. The samples were dried under vacuum at 80 °C for 24 h for characterization.

Characterization

The blends morphologies were examined by field emission scanning electron microscope (FESEM, JSM-6700, Japan). The cryo-fractured surface of samples in liquid nitrogen was etched by THF, and sputtered with gold before SEM examinations.

Transmission electronic microscopy (TEM) was carried out using a Hitachi H-800 microscope at an acceleration voltage of 90 kV. The samples were ultramicrotomed with a diamond knife on a Leica Ultra cut UCT microtomed at –20 °C to give nm thick sections.

X-ray diffraction (XRD) analysis was performed using a Rigaku D/Max-III X-ray diffraction analyzer equipped with a rotating-anode generator system using Cu K α ($\lambda = 1.5406 \text{ \AA}$) radiation at an operating current of 200 mA with 2θ varying between 2° and 30°. All experiments were carried out in a reflection mode at room temperature. The scanning speed was 1° min^{−1}, and step size was 0.05°.

A Waters-991 gel permeation chromatography (GPC) instrument was used to evaluate the number-average molecular weight (\bar{M}_n), weight-average molecular weight (\bar{M}_w), and their polydispersity indices (\bar{M}_w/\bar{M}_n) of MCPA6 microspheres and MCPA6 network phase, by calibration with a PA6 standard. The measurements were

performed at 35 °C on polymeric solutions in *m*-cresol ($c = 0.5 \text{ g dL}^{-1}$). All samples were dissolved by *m*-cresol and were filtered in order to remove the Na⁺-MMT, OMMT, and MMT-bound PA6. The MCPA6 in the filtrate was precipitated by acetone and dried under vacuum at 80 °C for 12 h.

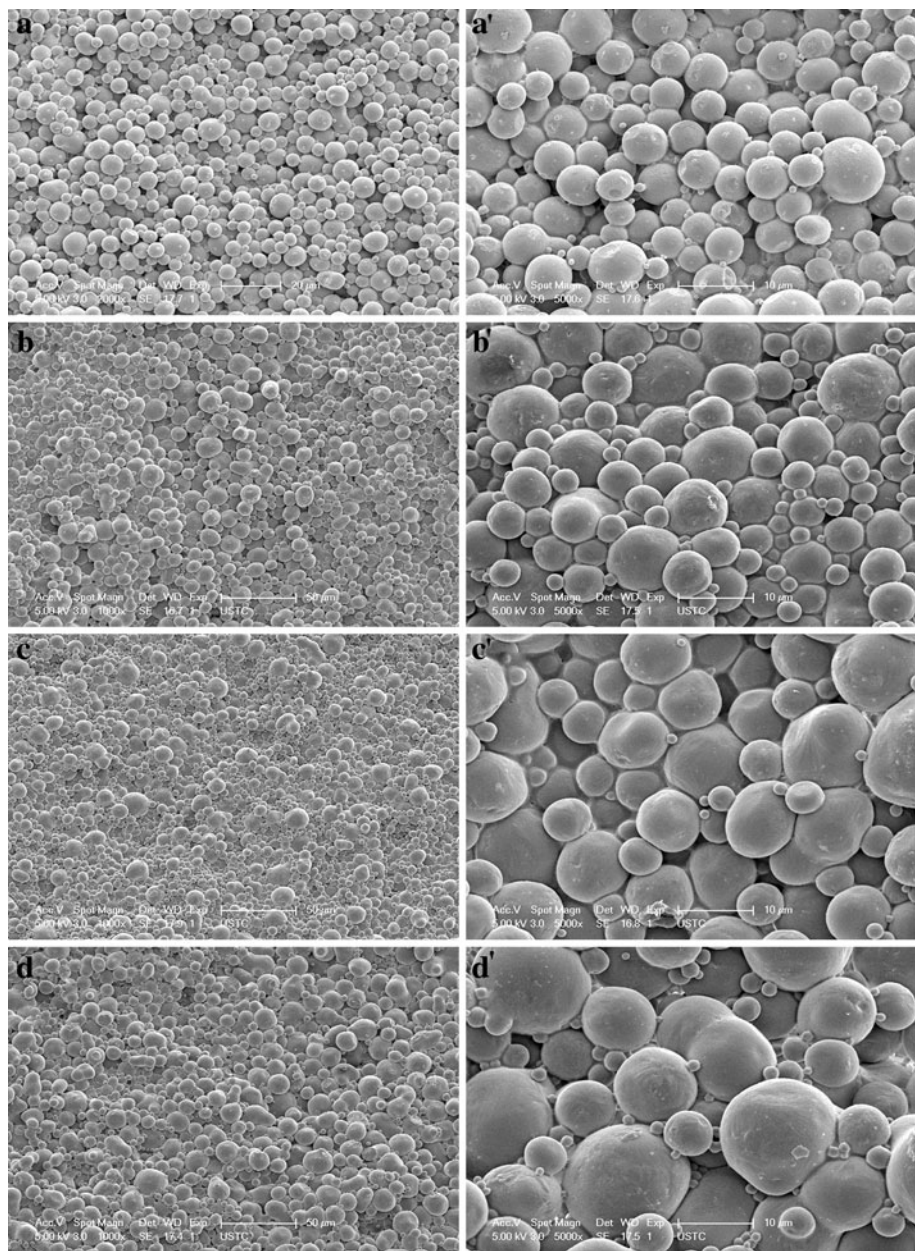
Differential scanning calorimeter (DSC) measurements were carried out using a NETZSCH DSC 200 PC calibrated by in standards. All the measurements were firstly performed from room temperature to 260 °C at a heating rate of 60 °C min⁻¹ under a nitrogen atmosphere and held for 5 min to remove any previous thermal history. Then it was cooling at 10 °C min⁻¹. A second heating scan was

carried out at 10 °C min⁻¹. The melting enthalpy (ΔH_f), which is a measure of crystalline degree, was used for comparison of the relative changes in the crystalline degree and the crystallinities of the MCPA6 microspheres and PA6 network phase were determined according to the following equation:

$$X_{\text{c},(\text{DSC})} = \Delta H_f / [(1 - \Phi) \times \Delta H_f^*] \times 100\%$$

where ΔH_f is the melting enthalpy of MCPA6 in the sample, Φ is the weight fraction of Na⁺-MMT and OMMT in the blends, and ΔH_f^* is the melting enthalpy of the matrix polymer of 100% crystallization [$\Delta H_f^* = 230 \text{ J g}^{-1}$] [29, 30].

Fig. 1 SEM micrographs of the cryo-fractured surfaces of Reference **a** NM0.5, **b** NM1, **c** NM2, **d** etched by THF and their corresponding magnifying images (**a'**–**d'**)



Results and discussion

SEM observation

Figures 1, 2, 3, and 4 show the SEM morphologies of MCPA6/PS and MCPA6/PS/MMT whose cryo-fractured surfaces are etched by THF. Figure 1 shows the morphologies of the binary blend and the composites NM0.5, NM1, and NM2. The blend without MMT shows a highly incompatible nature. The morphologies of PA6 dispersed/PS matrix are observed. By etched the PS continuous matrixes with THF, PA6 microspheres are obtained. The diameter of the spheres is about 5 μm . The morphologies of blends with various amounts of Na^+ -MMT (0.5, 1, and 2 wt%) show similar nature compared with that of binary blend. For MCPA6/PS/ Na^+ -MMT blends, the incorporation of a certain amount of Na^+ -MMT increased the domain diameter of PA6 microspheres to about 2–10 μm as shown in Fig. 1b-d. This result confirms the feasibility of the method for fabricating PA6/ Na^+ -MMT microspheres which combine the advantages of MCPA6 with natural MMT. However, SEM of Figs. 2, 3, and 4 reveals somewhat different phenomenon. The morphologies of the

MCPA6/PS/OMMT ternary blends depend strongly on the contents of OMMT. The morphology of OM0.5 is similar to binary blend (see Fig. 2). Once the OMMT content ≥ 1 wt%, phase inversion becomes imperfect, and the phase morphology of the ternary composites gradually changes from dispersed PA6 microspheres/PS matrix to PA6 network phase with inclusion of local dispersed PA6 microspheres/PS matrix structure.

Figures 3 and 4 show the co-existence phenomenon of PA6 microspheres and PA6 network structure. According to investigations on the formation mechanism of co-continuous structures by melt mixing, the process of morphology development likely involves the breakup processes of thin sheets of both components into a lacy-like structure and to fibrous filaments which can break up to droplets. These breakup mechanisms seem to be delayed by the OMMT layers since they enhance the viscosity of the filled component, as well as hinder the breakup of sheets or filaments mechanically [31, 32].

In this study, thermodynamics, kinetics, polymerization rates, and interaction between polymer chains and MMT layers are all competing factors that control the phase inversion of the in situ polymerization system during the polymerization of reactive solvent [33]. A wonderful phenomenon is also observed because of synergistic causes of above factors. When MMT is added into the MCPA6/PS blends, Na^+ -MMT is observed selectively locating in PA6 microspheres phase, while OMMT with content below 1% is observed in PA6 microspheres, OMMT with content great than or equal to 1 wt% is observed in PA6 network phase, not in PA6 microspheres phase.

To confirm the dispersion of OMMT in the blends, SEM-EDX spectra are conducted in OM1 and OM2. Figures 3e, f and 4e, f reveal the SEM-EDX spectra of PA6 microspheres region and PA6 network region of OM1 and OM2, respectively. It is inspiring that Silicon elements (MMT) are observed in PA6 network phase, not in PA6 microspheres. That is, OMMT only selectively located in PA6 network phase, not in PA6 microspheres (also see “TEM observation” section).

Chow et al. [34] have investigated the preferential intercalation behavior in the immiscible blend when one component was polar. Results show exfoliated clay platelets are selectively located in PA6 phase. This is in accordance with our results of SEM-EDX and TEM. The distribution of the MMT in the ternary blends will be described in detail in the TEM section. These observations suggest that the polarity of PA6 had a profound influence on the preferential intercalation behavior of MMT. In MCPA6/PS/MMT system, the high surface energy between MMT layers and PA6 polar amino-group leads to the high viscosity of the system, PA6 stronger affinity to MMT surfaces than PS.

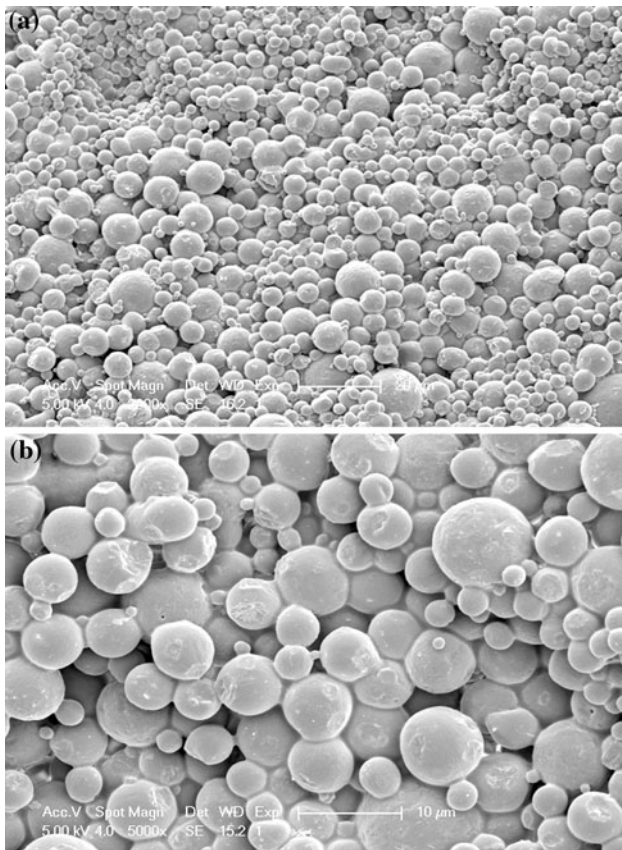
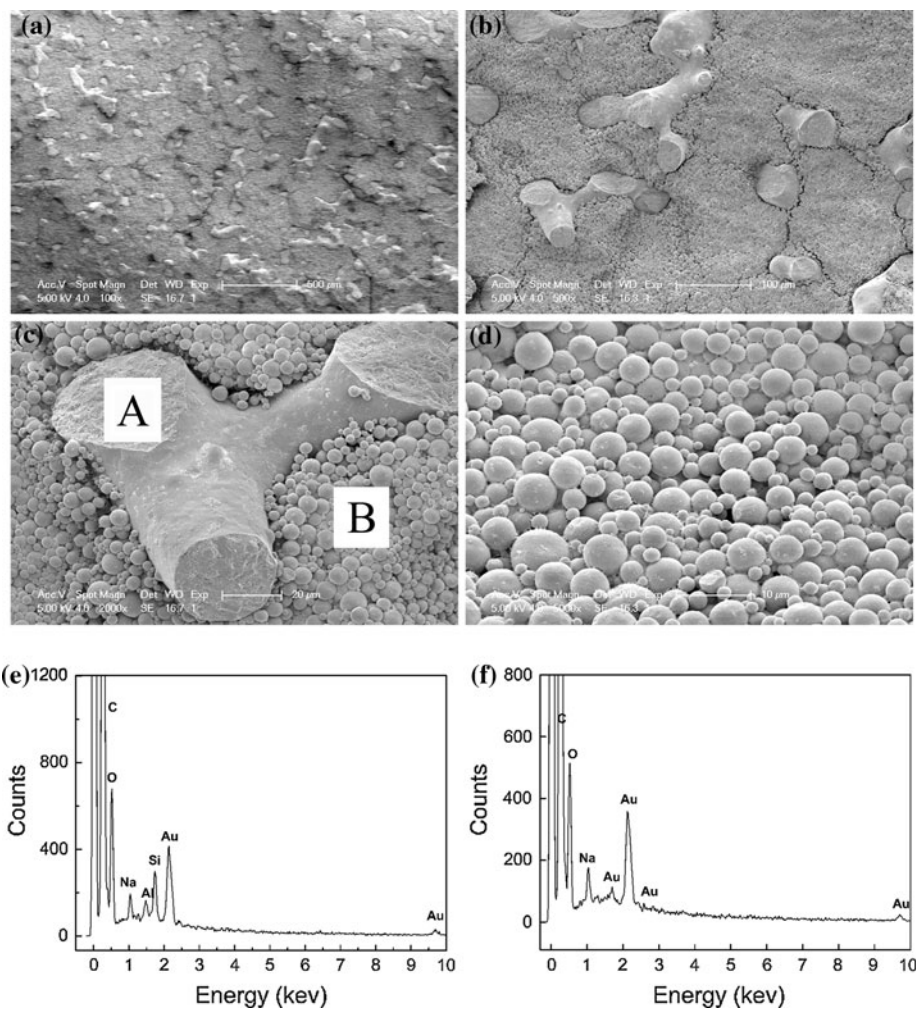


Fig. 2 SEM micrographs of the cryo-fractured surfaces of OM0.5 (a) etched by THF with its magnifying image (b)

Fig. 3 SEM micrographs of the cryo-fractured surfaces of OM1
(a) etched by THF with variously magnifying multiple
(b–d); SEM-EDX spectra of the OM1: **e** the spectrum corresponds to the A region in **(c)**, and **f** the spectrum corresponds to the B region in **(c)**



The morphology of MCPA6/PS/ Na^+ -MMT is different from MCPA6/PS/OMMT. Reasonable explanation is that the interaction between PA6 and Na^+ -MMT is stronger than that of OMMT. When the incorporation of Na^+ -MMT, sodium ion exchange with CL monomer easily, PA6 chains grow in the layers. The surface compatibility among them is stronger than that of OMMT. Thus, the Na^+ -MMT system forms PA6 microspheres structure. However, during polymerization of MCPA6/PS/OMMT, OMMT is intercalated with long-chain alkanes, stronger synergistic interaction among CL, PA6 chains, alkanes and OMMT layers leads to the viscous inhomogeneity of the blends. The phase inversion is obstructed in higher viscosity region during polymerization. PS flow matrix cannot completely break up the bulk of PA6, but exclude PA6 to form thin network structure. While in local lower viscosity region, phase inversion occurs to form dispersed PA6 microspheres/PS matrix. All the causes above create the wonderful morphologies of MCPA6/PS/OMMT. This study of phase separation creates possibilities for controlling

preparation of special morphologies impossible to obtain it via conventional method, such as melting mixing.

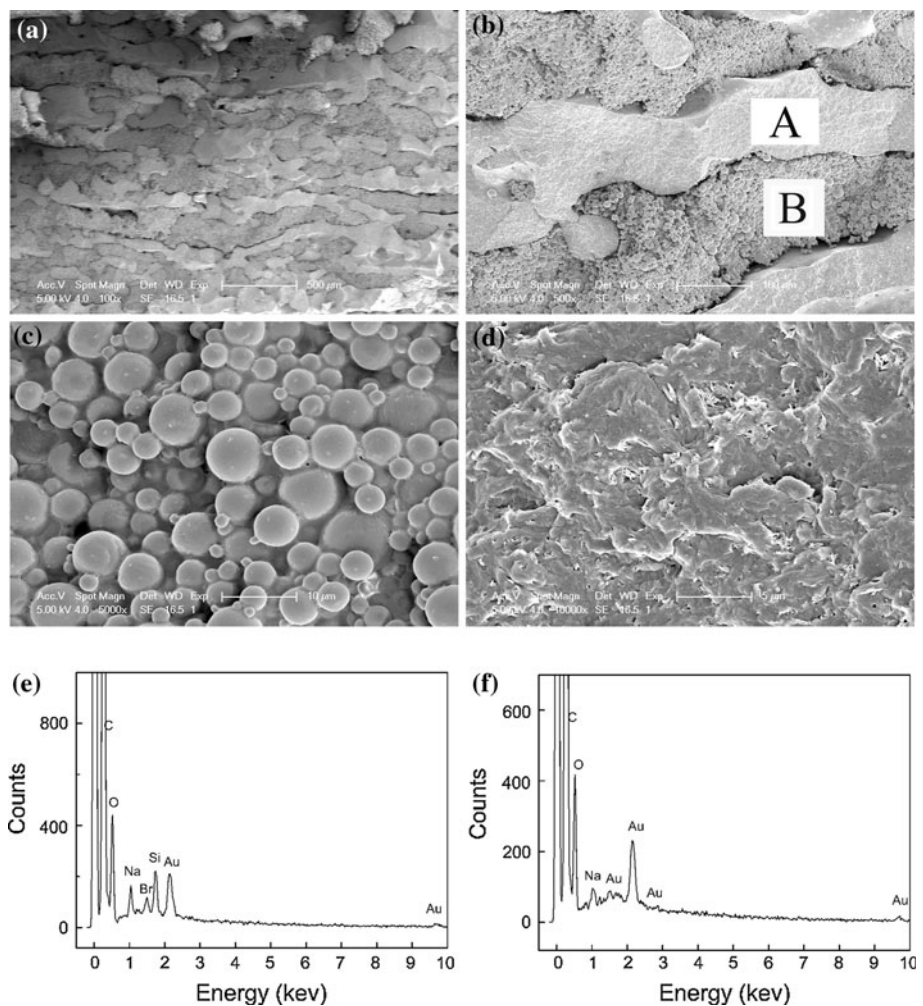
TEM observation

TEM is used to directly observe the MMT layers dispersion in the blends. TEM micrographs of NM2, OM0.5, and OM2 are shown in Fig. 5. Some separated dark lines (MMT layers) are distributed uniformly in PA6 microspheres (Fig. 5a–c) and PA6 network phase (Fig. 5d). In NM2 (Fig. 5a) and its magnifying image (Fig. 5b), Na^+ -MMT layers are clearly observed in PA6 microspheres. These results are related to selectively location of MMT in PA6 phase.

GPC results

The monomer conversion, \bar{M}_n , \bar{M}_w , and distributions (\bar{M}_w/\bar{M}_n) of MCPA6/PS and its ternary composites are given in Table 1 in order to evaluate the inhibiting effect of

Fig. 4 SEM micrographs of the cryo-fractured surfaces of OM2 (a) etched by THF with its magnifying multiple (b); (c, d) the magnifying images of region B and A of (b), respectively; SEM-EDX spectra of the OM2: e the spectrum corresponds to the A region in (b), and f the spectrum corresponds to the B region in (b)



Na^+ -MMT or OMMT on blends. From these results, it can be seen that the addition of Na^+ -MMT has no obvious effect on \overline{M}_w or $\overline{M}_w/\overline{M}_n$ of the blends, while a little effect on monomer conversion. This indicates that natural MMT has a little inhibiting role on blends. However, the monomer conversion and \overline{M}_n of microspheres of OM2 decrease comparing with that of network phase. Consequently, we can draw the conclusion that OMMT has a strong inhibiting role and leads to bad dispersion, which is consistent with Zhou's report [35].

Crystallization behavior

Figure 6 shows the XRD patterns of the ternary blends with various contents of Na^+ -MMT and OMMT. In Fig. 6a, Na^+ -MMT shows a peak at $2\theta = 7.60^\circ$, which correspond to basal spacing of 1.16 nm. However, the XRD pattern of NM0.5 shows no peaks within 10° , which demonstrates that Na^+ -MMT layers are delaminated. While the XRD of NM1 and NM2 shows a weak peak within 10° , corresponding to a co-existence of exfoliated and intercalated

structures. In Fig. 6b, similar phenomenon was observed when OMMT was added.

In addition, the crystallization behavior of MCPA6/PS and its ternary blends were investigated using XRD and DSC. In Fig. 6, peaks at about 20° and 23.6° can be assigned to the (200) and (002) planes of the α -phase, respectively. The peak around 21.5° is characterization of the γ -phase [(200) and (101) planes]. In MCPA6/PS/MMT systems, MMT plays a major role in the crystallization of the MCPA6/PS. From it, we can see that intercalated Na^+ -MMT or OMMT greatly change the behavior of crystallization of MCPA6/PS blends, prevent partially crystallization in the α -phase and lead to a sharp increase in the intensity of the γ -phase. In other words, the intercalated Na^+ -MMT or OMMT plays predominant effect to γ -crystalline form and minor effect to α -crystalline form. This may be due to the fact that intercalated MMT layers restricts mobility of the MCPA6 molecules chain, disturbs the perfect arrangement of hydrogen-bonded sheets of the α -phase, thus promoting the formation of the γ -phase [36, 37]. However, in Na^+ -MMT systems, a little difference can

Fig. 5 TEM micrographs of **a** NM2, **b** magnifying of (a), **c** OM0.5, and **d** OM2

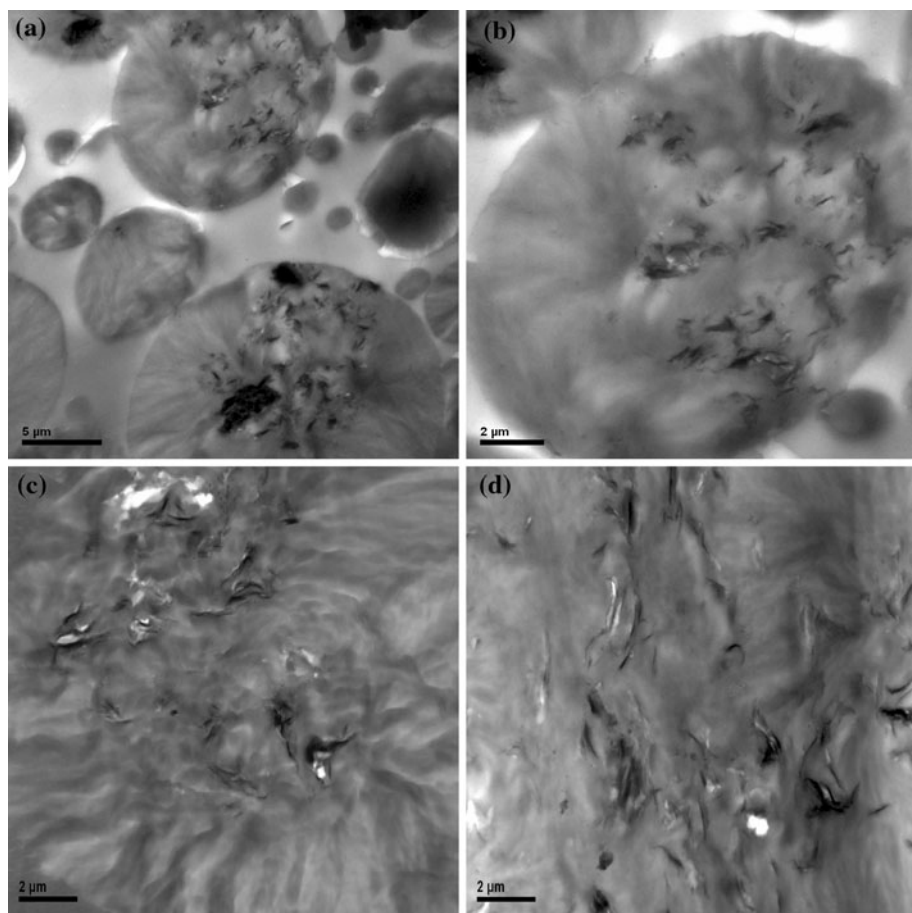


Table 1 \bar{M}_n , \bar{M}_w and polydispersity index(D) for PA6 microspheres and PA6 network phase

Sample	Conversion %	\bar{M}_n kg mol ⁻¹	\bar{M}_w kg mol ⁻¹	D \bar{M}_w/\bar{M}_n
PA6 microspheres	94	19.1	52.2	2.74
NM2% microspheres	92	18.7	42.1	3.01
OM0.5% microspheres	93	19.1	41.0	2.15
OM2% network phase	96	19.3	31.3	1.62
OM2% microspheres	94	15.1	28.2	1.88

still be found among their ternary composites. When Na⁺-MMT content is low (i.e., 0.5%), exfoliated MMT greatly change the behavior of crystallization of MCPA6, prevent crystallization in the α -phase and γ -phase. There is little effect with increase of contents. It is the fact that sodium ion is exchange with CL monomer during polymerization, the crystallization capacity and the ability to adopt its crystalline form of PA6 chains grown in the layers are inhibited [38]. OMMT layers are exchanged by alkanes, the dipole–dipole interactions between MMT, the ε -caprolactam monomer and alkanes prevent exfoliated MMT from restructuring into layers. While the hydrogen bond between the Na⁺-MMT and ε -caprolactam is unstable.

The Na⁺-MMT layers is prone to restructuring into layers. This results in Na⁺-MMT layers being transformed from an exfoliated structure into an intercalated structure. It is not strange that a γ -crystalline forms under lower Na⁺-MMT contents due to all the effects. The mechanism proposed here is based purely on assumption and elucidation of the exact mechanism will require further study.

The second heating and cooling thermograms of PA6 microspheres and the network phase of OM2 are shown in Fig. 7. The data are summarized in Table 2 in detail. The melt-crystallization behaviors are presented in Fig. 7a. The crystallization exothermal peaks of the ternary composites all shift to high temperature compared to neat PA6, which suggests that MMT, act as heterogeneous nucleating agent, increases the melt-crystallization temperature (T_c).

The second heating DSC traces are presented in Fig. 7b, in which peaks at about 204 and 214 °C are attributed to the melting peaks of the γ -crystalline form and the α -crystalline form of pure PA6 microspheres, respectively. When Na⁺-MMT is added, the peak intensity of T_{m1} develops. This is another evidence that nano-scale dispersed Na⁺-MMT layers favor the formation of the γ -crystalline form. But for MCPA6/PS/OMMT, different phenomenon is observed. The peak intensity of γ -crystalline form of PA6

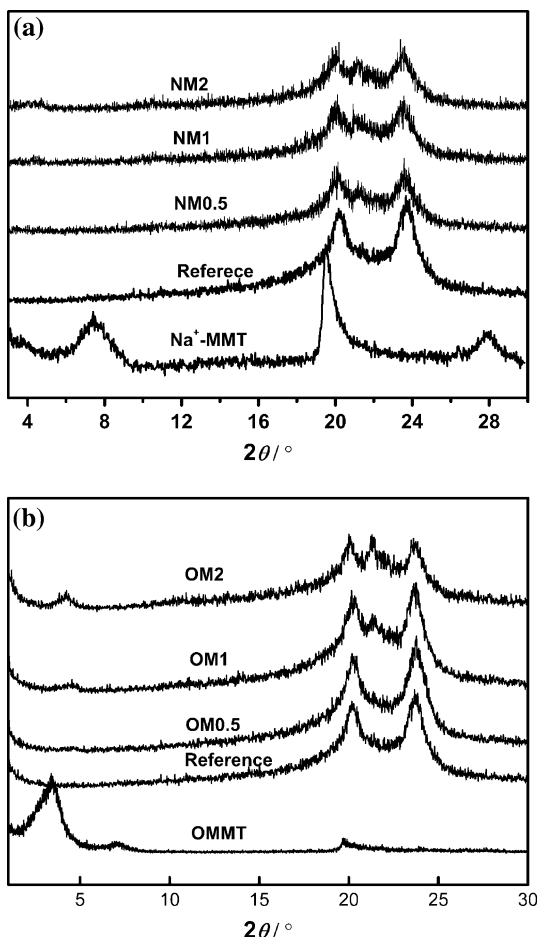


Fig. 6 The XRD patterns of **a** pristine Na^+ -MMT, **b** OMMT and their blends with various amounts of MMT

microspheres leads to much increase, while the peak intensity of γ -crystalline form of PA6 network phase is hardly strengthened. Additionally, the presence of well dispersed MMT does not alter the degree of crystallinity (X_c), as shown in Table 2. From the data in Table 2, another phenomenon is necessary to be mentioned. That is, the incorporation of OMMT increases the melt peak values of T_{m1} and T_{m2} of PA6 network phase. All of these are in good agreement with R. A. Vaia's results [39].

Conclusion

A novel method was used to directly synthesize MCPA6/PS/MMT ternary composites via successive in situ polymerization. In this system, DMAc was used as a pre-dispersant of Na^+ -MMT and OMMT to make MMT layers and PS/CL mixture mix well. SEM showed that the PA6 dispersed/PS matrix structure was changed when adding Na^+ -MMT or OMMT to the binary blend. The domain diameter of PA6 dispersed microspheres in the PS matrix

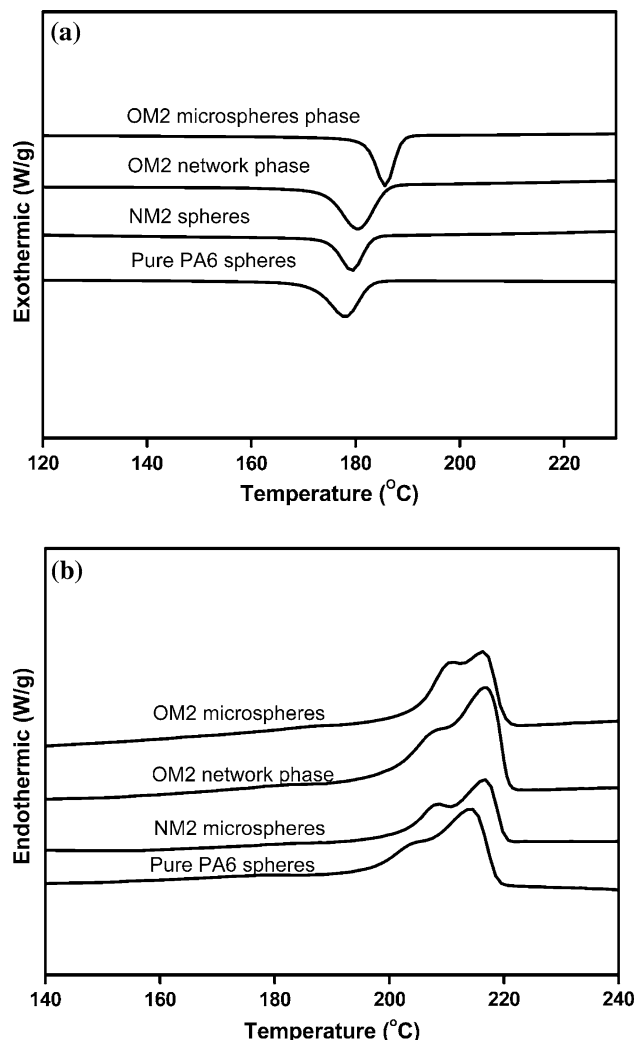


Fig. 7 DSC thermograms of PA6 phase with certain amounts of MMT **a** cooling and **b** the second heating

increased from several to dozens of micrometers with incorporation of certain content Na^+ -MMT. It was interesting to find that all Na^+ -MMT was dispersed only in the MCPA6 microspheres phase. However, a unique morphology was observed in PA6/PS/OMMT ternary blends, especially when the content of OMMT ≥ 1 wt%. That is, the morphologies of the blends changed from dispersed PA6 microspheres/PS matrix to dispersed PA6 network with inclusion of local PA6 microspheres dispersed/PS matrix. The results of TEM and SEM-EDX indicated that a small amount of OMMT (i.e., 0.5 wt%) dispersed in PA6 microspheres. At high OMMT loading (i.e., ≥ 1 wt%), OMMT was dispersed in PA6 network phase, not in PA6 microspheres phase. XRD revealed that Na^+ -MMT or OMMT promoted the forming of PA6 γ -crystalline due to the crystallization capacity and ability to adopt its crystalline form of PA6 chains were constrained. DSC results showed that the incorporation of Na^+ -MMT result in peak

Table 2 Characteristic values of crystallization and melting behavior of PA6 spheres and its spheres with certain amounts of MMT

Sample	Heating (second)				Cooling		
	T_{m1} °C	T_{m2} °C	ΔH_f J g ⁻¹	$X_c(DSC)$ %	ΔH_c J g ⁻¹	$W_{1/2}$ °C	T_c °C
MCPA6 microspheres	204.3	214.1	45.5	19.8	49.8	9.1	177.9
NM2 microspheres	210.2	216.2	42.0	18.6	45.1	6.6	180.5
OM2 microspheres	207.8	216.2	42.7	18.9	47.9	6.6	185.6
OM2 network phase	208.4	216.9	44.6	19.8	44.4	8.6	180.8

intensity of PA6 γ -crystalline increased somewhat. OMMT had weaker effect in increasing peak intensity of γ -crystalline of PA6 network phase compared with that Na⁺-MMT. Another interesting phenomenon was that there was a remarkable difference of molecular weight of PA6 microspheres phase and PA6 network phase in OM2 ternary composites from GPC results.

References

- Gawad AA, Esawi AMK, Ramadan AR (2010) J Mater Sci 45:6677. doi:[10.1007/s10853-010-4760-5](https://doi.org/10.1007/s10853-010-4760-5)
- Mohan TP, Ramesh Kumar M, Velmurugan R (2006) J Mater Sci 41:2929. doi:[10.1007/s10853-006-5164-4](https://doi.org/10.1007/s10853-006-5164-4)
- Giannelis EP, Krishnamoorti R, Manias E (1999) Adv Polym Sci 138:107
- Kojima Y, Usuki A, Kawasumi M, Okada A, Fukushima Y, Kurauchi T et al (1993) J Mater Res 8:1185
- Usuki A, Kojima Y, Kawasumi M, Okada A, Fukushima Y, Kurauchi T et al (1993) J Mater Res 8:1179
- Kawasumi M (2004) J Polym Sci A 42:819
- Fornes TD, Yoon PJ, Hunter DL, Keskkula H, Paul DR (2002) Polymer 43:5915
- Ma J, Yu ZZ, Zhang QX, Xie XL, Mai YW, Luck I (2004) Chem Mater 16:757
- Yeh JM, Liou SJ, Lai CY, Wu PC, Tsai TY (2001) Chem Mater 13:1131
- Cho JW, Paul DR (2001) Polymer 42:1083
- Fornes TD, Yoon PJ, Hunter DL, Keskkula H, Paul DR (2001) Polymer 42:9929
- Chen BQ, Evans JRG (2004) J Phys Chem B 108:14986
- Liu Y, Chen ZM, Yang GS (2010) J Mater Sci Online First™, 25 August
- Li YL, Yang GS (2010) J Mater Sci 45:987. doi:[10.1007/s10853-009-4029-z](https://doi.org/10.1007/s10853-009-4029-z)
- Gong Y, Yang GS (2009) J Mater Sci 44:4639. doi:[10.1007/s10853-009-3708-0](https://doi.org/10.1007/s10853-009-3708-0)
- Kim DH, Park KY, Kim JY, Suh KD (2000) J Appl Polym Sci 78:1017
- Park SH, Park KY, Suh KD (1998) J Polym Sci B 36:447
- Park CD, Jo WH, Lee MS (1996) Polymer 37:3055
- Guo TY, Song MD, Hao GJ, Zhang BH (2001) Eur Polym J 37:241
- Jannasch P, Wesslén B (1998) J Appl Polym Sci 70:1887
- Rodríguez Ríos H, Nuño-Donlucas SM, Puig JE, González-Núñez R, Schulz PC (2004) J Appl Polym Sci 91:1736
- Villarreal ME, Tapia M, Nuño-Donlucas SM, Puig JE, González-Núñez R (2004) J Appl Polym Sci 92:2545
- Pei AH, Liu AD, Xie TX, Yang GS (2006) Macromolecules 39:7801
- Godjevargova T, Nenkova R, Dimova N (2005) Macromol Biosci 5:760
- Darkow R, Groth T, Albrecht W, Lützow K, Paul D (1999) Biomaterials 20:1277
- Yalcin G, Elmas B, Tuncel M, Tuncel A (2006) J Appl Polym Sci 101:818
- Hu J, Li SJ, Liu BL (2006) Biotechnol J 1:75
- Bahar T, Tuncel A (2000) React Funct Polym 44:71
- Evstatiev M, Schultz JM, Petrovich S, Georgiev G, Fakiov S, Friedrich K (1998) J Appl Polym Sci 67:723
- Liu AD, Xie TX, Yang GS (2006) Macromol Chem Phys 207:2180
- Khare RA, Bhattacharyya AR, Kulkarni AR, Saroop M, Biswas A (2008) J Polym Sci B 46:2286
- Pötschke P, Bhattacharyya AR, Janke A (2003) Polymer 44:8061
- Cui J, Yu Y, Chen W, Li S (1997) Macromol Chem Phys 198:3267
- Chow WS, Ishak ZAM, Karger K (2005) J Macromol Mater Eng 290:122
- Liu MG, Song Q, Zhou CX (2004) In: Proceeding of 2004 National Symposium of Polymer Materials Science and Engineering, China, p 241
- Liu AD, Xie TX, Yang GS (2006) Macromol Chem Phys 207:701
- Liu AD, Xie TX, Yang GS (2006) Macromol Chem Phys 207: 1174
- Lee DC, Jang LW (1996) J Appl Polym Sci 61:1117
- Lincoln DM, Vaia RV (2004) Macromolecules 37:4554